Sub-seasonal soil moisture anomaly forecasting using combinations of deep learning, based on the reanalysis soil moisture records

Wang, Xiaoyi; Corzo, Gerald; Lü, Haishen; Zhou, Shiliang; Mao, Kangmin; Zhu, Yonghua; Duarte, Santiago; Liu, Mingwen; Su, Jianbin

DOI
10.1016/j.agwat.2024.108772

Publication date
2024

Document Version
Final published version

Published in
Agricultural Water Management

Citation (APA)
Wang, X., Corzo, G., Lü, H., Zhou, S., Mao, K., Zhu, Y., Duarte, S., Liu, M., & Su, J. (2024). Sub-seasonal soil moisture anomaly forecasting using combinations of deep learning, based on the reanalysis soil moisture records. *Agricultural Water Management*, *295*, Article 108772. https://doi.org/10.1016/j.agwat.2024.108772

Agricultural Water Management 295 (2024) 108772

Contents lists available at ScienceDirect

Agricultural Water Management

journal homepage: www.elsevier.com/locate/agwat

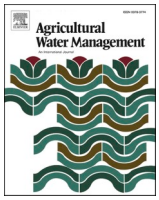

Sub-seasonal soil moisture anomaly forecasting using combinations of deep learning, based on the reanalysis soil moisture records

Xiaoyi Wang [a,b], Gerald Corzo [c], Haishen Lü [b,d,*], Shiliang Zhou [a], Kangmin Mao [e], Yonghua Zhu [b,d], Santiago Duarte [c,e], Mingwen Liu [b,d], Jianbin Su [f]

[a] Southwest Research Institute for Hydraulic and Water Transport Engineering, Chongqing Jiaotong University, Chongqing 400074, China
[b] State Key Laboratory of Hydrology-Water Resources and Hydraulic Engineering, National Cooperative Innovation Center for Water Safety and Hydro-science, College of Hydrology and Water Resources, Hohai University, Nanjing 210098, China
[c] Hydroinformatics Chair Group, IHE Delft Institute for Water Education, Delft 2611AX, the Netherlands
[d] Joint International Research Laboratory of Global Change and Water Cycle, Hohai University, Nanjing 210098, China
[e] Faculty of Civil Engineering and Geosciences, Delft University of Technology, Delft, the Netherlands
[f] National Tibetan Plateau Data Center, Key Laboratory of Tibetan Environmental Changes and Land Surface Processes, Institute of Tibetan Plateau Research, Chinese Academy of Sciences, Beijing, China

ARTICLE INFO

Handling Editor - J.E. Fernández

Keywords:
Drought forecasting
Deep learning
Committee model
Reanalysis soil moisture
Noise-assisted tool

ABSTRACT

Sub-seasonal drought forecasting is crucial for early warning in estimating agricultural production and optimizing irrigation management, as forecasting skills are relatively weak during this period. Soil moisture exhibits stronger persistence compared to other climate system quantities, which makes it especially influential in shaping land-atmosphere feedback, thus supplying a unique insight into drought forecasting. Relying on the soil moisture memory, this study investigates the combination of multiple deep-learning modules for sub-seasonal drought indices hindcast in the Huai River basin of China, using long-term ERA5-Land soil moisture records with a noise-assisted data analysis tool. The inter-compared deep-learning models include a hybrid model and a committee machine framework. The results show that the performance of the committee machine framework can be improved with the help of series decomposition and the forecasting skill is not impaired with the lead time increases. Overall, this study highlights the potential of combining deep-learning models with soil moisture memory analysis to improve sub-seasonal drought forecasting.

1. Introduction

Droughts significantly damage both nature and human society, especially in agriculture which relies heavily on water resources and soil moisture throughout crop growth, and even more so in developed countries than in developing ones (Lesk et al., 2016; Narasimhan and Srinivasan, 2005). Given the deep impact of droughts on crop security, forecasting it constitutes a major challenge in the fields of water resources and environmental engineering. The chaotic nature of weather patterns and the time needed to take action contrasts with the need to continuously analyze different components of the system (Araghinejad et al., 2017). The most damaging droughts are those that evolve quickly, leaving little time for stakeholders to implement proactive measures. For example, the drought in US Midwest during the summer of 2012 rapidly depleted soil moisture in the root zone, leading to severe soil drought within just two months. In many areas, the drought severity increased by three levels within one month, meaning a rapid transition from a normal state at the beginning of the month to a severe drought by month-end (Hoerling et al., 2014). An analysis by Gou et al. (2022) on sudden-onset droughts in the Huaibei Plain, a major grain-producing region in China, found that these events occurred most frequently in the northeastern and western regions of the plain. Across the area, the average occurrence frequency is 18 events per 19 years, with an average duration of about 31 days. Importantly, in situations of rapid and widespread sudden-onset drought changes, obtaining timely warnings using existing drought forecast products becomes challenging, but the products often focus on a seasonal scale and may be updated only on a monthly basis (Otkin et al., 2015). Therefore, there is an urgent need for

* Corresponding author at: Southwest Research Institute for Hydraulic and Water Transport Engineering, Chongqing Jiaotong University, Chongqing 400074, China.
E-mail address: lvhaishen@hhu.edu.cn (H. Lü).

https://doi.org/10.1016/j.agwat.2024.108772
Received 22 February 2023; Received in revised form 6 March 2024; Accepted 9 March 2024
Available online 13 March 2024

a sub-seasonal, frequently updated drought early warning system (Lorenz et al., 2018).

Changes in soil moisture reflect the combined effects of climate, vegetation, and soil processes (Esit et al., 2021). Previous studies have found that the persistence of soil moisture is closely related to the climate system. This is because soil moisture affects the distribution of surface latent heat flux and sensible heat flux, thereby influencing near-surface atmospheric conditions, boundary layer stability, and precipitation (Ford et al., 2015; Seneviratne et al., 2010). Chatterjee et al. (2022) demonstrated the leading role of soil moisture in controlling ecosystem dryness and confirming "drought memory", possibly due to the soil moisture memory in the land-atmosphere coupling, which sets prerequisites for the predictability of soil moisture. Top-layer soil responds fast to meteorological anomalies and serves as a sensitive drought indicator (Dorigo et al., 2012). Soil moisture anomaly percentage index (SMAPI), which is based exclusively on soil moisture with minimum complexity in a calculation, reflects the degree of saturation or dryness of the soil compared to normal conditions and is qualified to evaluate the effect of recent moisture conditions on crops (Bergman et al., 1988). SMAPI is highly beneficial in quantifying agricultural drought conditions over the regional and global long-term soil moisture information (Liu et al., 2019, 2021; Mao et al., 2017).

The prediction of soil moisture has long been hindered by insufficient observations. In recent years, with the increase in the deployment of ground stations, such as the International Soil Moisture Observation Network (Dorigo et al., 2021), and the surge in earth observation data, researchers have shown a great interest in adopting data-driven techniques. Data-driven techniques offer the advantage of directly extracting information from large-scale observational data and learning complex patterns. In contrast to traditional physical models, data-driven approaches do not require extensive prior knowledge but instead derive implicit patterns from the data itself. The deep learning (DL) methods sourced by Artificial Neural Networks (ANN) have good performance in dealing with nonlinear problems and pave the way for multidiscipline with great success. Typically, a single DL architecture is defined as a solo DL, while the model is called a hybrid DL model when two DL models are connected or cascaded (Meng et al., 2020). The hybrid models tend to show more stable and superior performance than solo DL models (Jena et al., 2021). In soil moisture and its derived drought forecasting, researchers tend to use multiple inputs, such as atmospheric factors and surface parameters (including soil information), for modeling. Commonly used solo forecasting frameworks include LSTM (Li et al., 2022b), extreme learning machine (ELM) (Prasad et al., 2018), Random Forest (Prasad et al., 2019b), Artificial Neural Network, Support Vector Machine (SVM) (Dubois et al., 2021)and so on, As for hybrid forecasting models, the models coupling CNN with other solo models are prevalent (Ahmed et al., 2021; Koné et al., 2023; Yu et al., 2021). Moreover, it is essential to note the CNN-LSTM hybrid model architecture, as it has recently demonstrated its effectiveness in meteorological drought forecasting (Adikari et al., 2021; Danandeh Mehr et al., 2022; Dikshit et al., 2022). Nevertheless, a limitation of both solo DL and the hybrid model is that only the best network is selected and the rest are discarded, potentially wasting networks with generalizations (Bullinaria, 2004). In response to this problem, committee machines were proposed when the individual members have low bias and are decorrelated (Hu and Hwang, 2002), and its own parallelism comes at little extra cost (Joksas et al., 2020). Specifically, the committee model requires partitioning data in relation to such processes using the available domain knowledge or expert judgment, then developing independent models for each process in parallel, and integrating them into a modular model (Corzo and Solomatine, 2007).

It should be considered that the input series to the data-driven model are often non-stationary, hence data decomposition has become an effective pre-processing method to extract trends and harmonics and remove noise from non-stationary time series (Wu et al., 2010), e.g., principal component analysis (PCA), singular spectrum analysis (SSA), wavelet analysis (WA), Gamma test (GT), etc. Such pre-processing approaches strengthen the forecasting skill in predicting nonlinear issues. Ensemble Empirical Mode Decomposition (EEMD) proposed by Wu and Huang (2009) is a new and promising approach for decomposing time series data. It is an empirical, intuitive, and self-adaptive method with few parameters to set and has the ability to work locally in both physical and frequency space. Especially when EEMD is combined with committee models, the accuracy of related soil moisture-related forecasts is significantly improved, e.g., Prasad et al. (2019a) proposed a multivariate sequential EEMD scheme to address naturally embedded non-stationary features within multivariate hydro-meteorological predictor inputs in forecasting weekly soil moisture in the selected 4 sites in New South Wales, Australia. Similarly, Prasad et al. (2018) integrated an ELM with EEMD to successfully forecast upper (0.2 m) and lower soil moisture (0.2–1.5 m) at the same four sites.

However, current forecasting models primarily operate at the point scale, relying heavily on extensive meteorological and land surface data. This limitation not only restricts their ability to capture large-scale spatial variations in soil moisture but also poses challenges in applying them to data-poor regions, limiting their generalization to diverse locations and larger basin scale. Moreover, the temporal resolution of relevant forecasting products is mostly at a monthly scale, limiting the detailed observation of soil moisture changes, especially in scenarios requiring timely decision-making for rapidly evolving drought events. Additionally, compared to other meteorological or hydrological variables, data-driven techniques have not yet been fully exploited in the field of soil moisture prediction in general.

Inspired from the foundational understanding of soil moisture memory and the significant role of series decomposition in short-term soil moisture forecasting, this study explores the possibility of sub-seasonal drought index hindcasting using multi-DL frameworks and exclusively relying on soil moisture records. This is achieved by employing a multi-year ERA5-Land hourly soil moisture dataset under various DL frameworks. To avoid underfitting or overfitting issues in a solo or hybrid DL model, an ensemble committee framework is introduced, together with a hybrid model-CNN-LSTM, which delivers outstanding skills in meteorological drought works, which we select as a comparison. The process begins with pre-processing the weekly soil moisture anomaly index (SMAI) transformed by ERA5-Land soil moisture records using the EEMD technique. Then, both the committee model and the hybrid CNN-LSTM model are applied in parallel for forecasting the next 1–4 weeks of subcomponents. Finally, we evaluate the integrated datasets with sorted lead times against the SMAI series derived from ERA5-Land using continuous and categorial validation.

2. Study area and materials

2.1. Study area

The testing area named the Huai River basin (HRB, Fig. 1) is located in middle eastern China with an area of 270,000 km^2 and a population of 165 million inhabitants with great socio-economic potential (He et al., 2015). It generally has a humid and sub-humid warm-temperature monsoon climate (Zheng et al., 2021). The average annual temperature in the HRB is between 11 and 16 °C, and the actual evaporation there is between, 900–1500 mm. The average annual precipitation is characterized by a distinctive spatio-temporal distribution increasing from the northwest (600 mm) to the southeast (1000 mm) - with a basin average of 888 mm (Pan et al., 2018).

Besides, the HRB takes up 20 percent of the total agricultural production with 10 percent of the total cropland of China, feeding 20.4 percent of the total rural population (Sun et al., 2017). Approximately 80 percent of the land is heavily cultivated (statistic from the C3S-LC-L4-LCCS-Map-300 m-P1Y-2020-v2.1.1 land cover map), and one-third of the HRB requires irrigation (Wang et al., 2021). As a representative region prone to drought, frequent droughts in the HRB

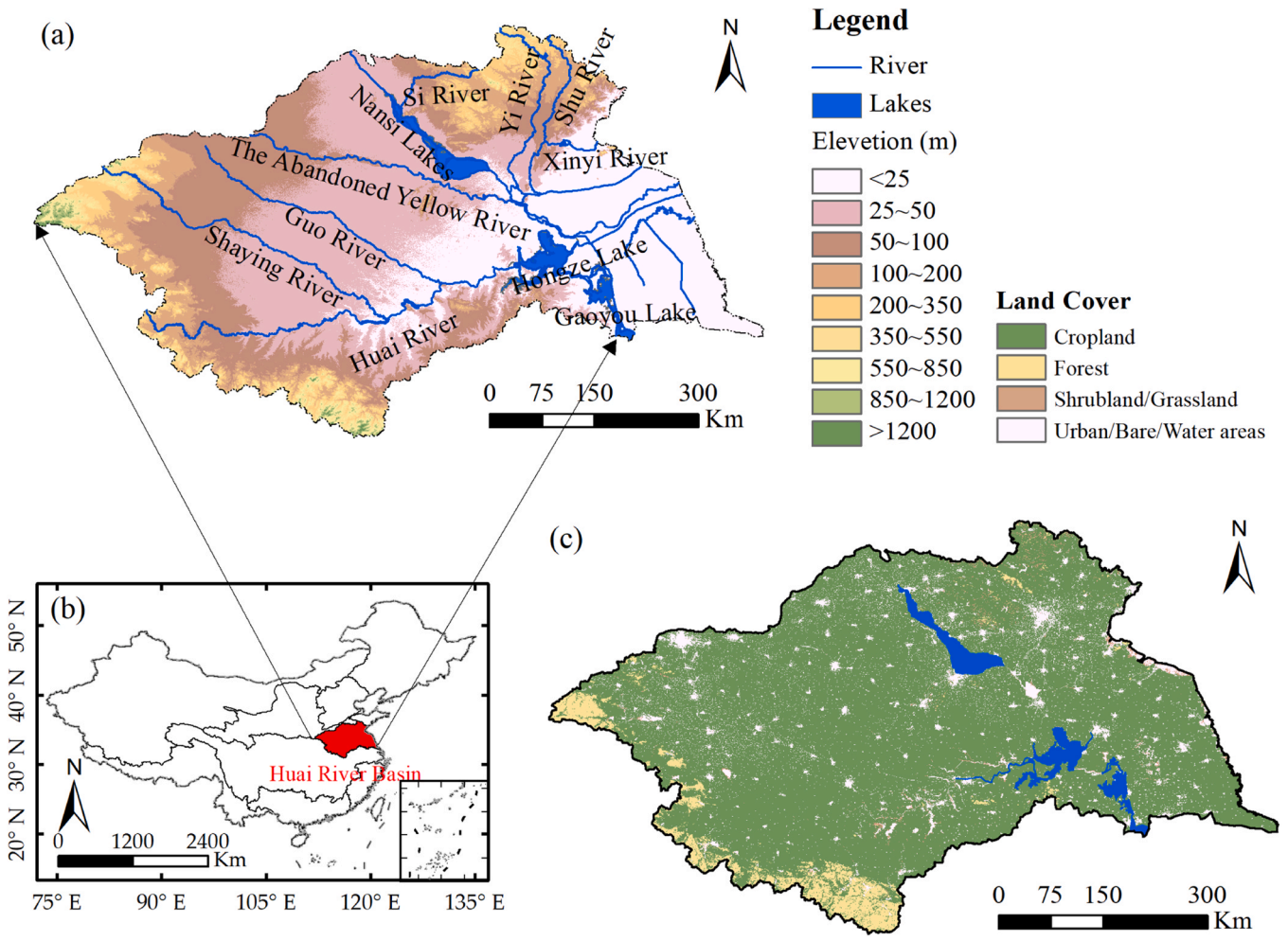

Fig. 1. The elevation information of the HRB (a), its position in China (b), and the land cover map over the HRB (c).

have substantial negative impacts on local agricultural production (Zhang et al., 2012, 2019).

2.2. Materials

2.2.1. ERA5-Land hourly volumetric soil moisture data

The ERA5-Land, released by the European Centre for Medium-Range Weather Forecasts (ECMWF), is producing an enhanced global dataset for the land component of the fifth generation of European ReAnalysis (ERA5) (Muñoz-Sabater et al., 2021). In contrast to ERA5, the development of ERA5-Land is not coupled to the atmospheric module of the ECMWF Integrated Forecast System (IFS) and therefore can be updated quickly without data assimilation (Wu et al., 2021). The ERA5-Land soil moisture datasets have proven to be effective and reliable in delivering precise soil moisture information, as demonstrated by a comparison with in-situ measurements (Zheng et al., 2022). In particular, a recent assessment in Jiangsu Province within the HRB found that ERA5-Land outperforms other main land surface model outputs and active/passive remote sensing observations in terms of accuracy (Fan et al., 2022).

This research selected the volumetric soil water layer 1 (0–7 cm) with 0.1° × 0.1° grids spacing of ERA5-Land as the real weather proxy, and the collection period is from 1979 to 2020 with a reduced temporal resolution of natural week processed by averaging hourly data.

2.2.2. Soil Moisture of China by in situ data, version 1.0 (SMCI1.0)

SMCI1.0 is a multi-layer (10 layers with 10-centimeter intervals from 10 to 100 cm) long-term (2000–2020) seamless daily dataset with high resolution and minimal errors (Li and Zhang, 2023; Li et al., 2022a). This dataset was constructed through a designed Random Forest model trained on 1789 in-situ soil moisture measurements operated by China Meteorology Agency. After underwent rigorous assessment through a station-to-station evaluation against in-situ soil moisture data, SMCI1.0 exhibited ubRMSE (0.045–0.051 m^3/m^3), MAE (0.035 m^3/m^3), R (0.866–0.893), and R^2 (0.749–0.798). Meanwhile, a 9 km resolution iteration version, which can be accessed on National Tibetan Plateau Data Center (Shangguan, 2023), was generated by aggregating higher-resolution predictor variables, catering to the needs of large-scale research requiring coarser soil moisture. Overall, SMCI1.0 generally demonstrates advantages over other gridded soil moisture products in China, including ERA5-Land, SMAP-L4, and SoMo.ml. SMCI has also applied in gridded soil moisture inter-comparison (Zhao et al., 2023) and a series of applications related with soil moisture (Li and Zhang, 2023; Yu et al., 2023; Zhao et al., 2023)

Before initiating the modeling process, we assess the surface soil moisture records of ERA5-Land at daily scale using the 9 km resolution SMCI1.0 first-layer soil moisture data (0–10 cm) as the reference dataset, spanning from 2000 to 2020.

2.2.3. ECMWF land cover classification gridded map

Since the HRB is a cropland-dominated area, the land cover map helps the study find the prediction performance in cropland. Out of the consistency of the data, the land cover map used here is derived from ECMWF Copernicus Climate Data Store. The land cover maps for 2016–2020 are based on satellite observations including Project for On-

Board Autonomy-Vegetation and Sentinel 3 - Ocean Land Color Instrument (OSCI) satellites and are consistent with the existing Climate Change Initiative global annual LC maps from 1992 to 2015. The related maps have a resolution of 300 m for 2016–2020 (version 2.1). The Coordinate Reference System used for the global land cover database is a geographic coordinate system (GCS) based on the World Geodetic System 84 (WGS84) reference ellipsoid.

3. Methods

This section describes the details about the methods embedded in the forecasting framework in this study.

3.1. Soil Moisture Anomaly Index (SMAI)

SMAPI is used to define drought severity through a measurement of the relative departure of soil moisture from the normal climate at a specific grid (Wu et al., 2011). SMAI is a simplified form of SMAPI that ignores the percentage component in the calculation, referred to Eq. 1:

$$SMAI = \frac{(\theta - \bar{\theta})}{\bar{\theta}} \quad (1)$$

Where θ and $\bar{\theta}$ represent the weekly soil moisture and its climatology (multi-year average) separately at each grid. Referred to the defined criteria of SMAI classification, agricultural drought is indicated by a soil water content anomaly when SMAI is less than −0.05. The drought severity can be referred the Table 1 below.

In this study, the weekly average soil moisture records from ERA5-Land are first converted into weekly SMAI signals (denoted as ERA5L-SMAI), thus serving as the next step in mode $_{\text{decomposition}}$.

3.2. Ensemble empirical mode decomposition

The EEMD technique proposed by (Wu and Huang, 2009) is a data analysis technique that decomposes complex signals into a set of intrinsic mode functions (IMFs) and residuals by adding white noise to the data series. The aim of using EEMD is to improve the robustness of the limited decomposed signal by averaging the results from a large number of trials. The process of EEMD implementation involves adding white noise to the data series, then decomposing the signal into a fixed number of IMFs and residuals. In this study, for each grid (out of the 2597 grids included), the EEMD process is set to 100 trials and the resulting decomposed signals are fixed to 6 IMFs and 1 residual.

1) Add white noise to the original signal *x(t)* and set the noise width dynamically in line with the standard deviation of the original sequence, Gaussian noise.
2) Set the number of parallel trails and start sequence decomposition by confirming the local maximum and minimum values.
3) Connect all local maxima and local minima separately and use spline interpolation to obtain upper and lower envelopes ($e_{max}(t)$ and $e_{min}(t)$).
4) Calculate the mean of the upper and lower envelopes.
5) Computes the difference *diff(t)* between the original series *x(t)* and the mean envelope $\bar{e}(t)$.
6) Determine whether *diff(t)* satisfies the two conditions of the above IMF, if so, continue to step 7, otherwise, *diff(t)* will be assigned to *x(t)*, and repeat steps 2–6.
7) Save *diff(t)* to the IMF set, and then update the data sequence in step 1 to the remainder $r(t) = x(t) - diff(t)$, repeat steps 1–6 until *r(t)* is a monotonic function or has at most one local extremum point, then stop the decomposition process and save *r(t)* as a separate residue term.
8) The mean of the IMFs and residuals decomposed under parallel experiments is calculated as the final result.
9) After obtaining all *n* mean IMFs and their residues, the original data sequence *x(t)* can be expressed as the Eq. 2:

$$SMAI(t) = \sum_{i=1}^{n} IMF_i(t) + r(t) \quad (2)$$

Where $IMF_i(t)$ is the i_{th} IMF obtained from EEMD, and *r(t)* represents the mean of the total corresponding residues at *t* moment.

Table 1
Drought classification for SMAI.

Drought level	SMAI
Drought-free	> 0.05
Mild drought	- 0.15 ~ 0.05
Moderate drought	- 0.3 ~ −0.15
Severe drought	< −0.3

3.3. DL-based committee forecasting tool

The committee machine used in this study is amalgamating K-parallel recurrent neural networks (KRNN), convolutional neural networks (CNN), graph convolutional networks (GCN), and multi-layer perceptron (MLP). Such submodules are combined, designed as three independent composite models running autonomously, respectively are KRNN, MLP, and a “Sandwich” model. The forecasting stage discards any models with a validation loss higher than the sum of the minimum and standard deviation of all submodules’ validation losses, while the predictions of the remaining submodules are averaged to obtain the final forecasts. This integrated model is encapsulated in Pytorch-based the Forecasting Open Source Tool (FOST), developed by Microsoft Research Asia and available on GitHub [https://github.com/microsoft/FOST]. The process is illustrated in Fig. 2a.

The three key modules of the design run independently before the output results, and their structures are as follows. The KRNN allows multiple parallel-operated RNN models to encode inputs to capture long-term correlations. These RNN encoders are equipped with an attention mechanism to ensure a weighted average for each node, capturing local and long-term correlations at the node level. Spatial weights between training targets (grids) are pre-loaded into the model during configuration to assist KRNN in capturing data features. The MLP component is a fully connected multi-layer neural network with residual connections with processing input data to obtain predictions iteratively. The "sandwich" model in FOST sequentially connects mixed models, incorporating a mixed CNN-KRNN model, a GCN model (GATNet), and another CNN-KRNN for updated features, allowing selective transmission of spatial weight information in each sub-model. Like KRNN, the "sandwich" model allows selective transmission of spatial weight information in each sub-model, sharing weight matrices with KRNN.

In operations, normalization is applied to the original (for the naive model) and the EEMD-decomposed sequences. Training data spans January 1980 to February 2019 (2043 weeks), with a testing period from March 2019 to December 2020 (97 weeks). Training sets have internal training and validation set ratios of 3:1, 5:1, and 7:1, using mean square error (MSE) as the loss function. Spatial weights for KRNN and the sandwich model are assigned using a simple method based on the surrounding weight matrix of the central pixel. Taking a grid needing allocation as an example (Eq. 3), the surrounding weight matrix of the central pixel can be computed, where s_c is the center value and s_i denotes the pixel value (gridded SMAI).

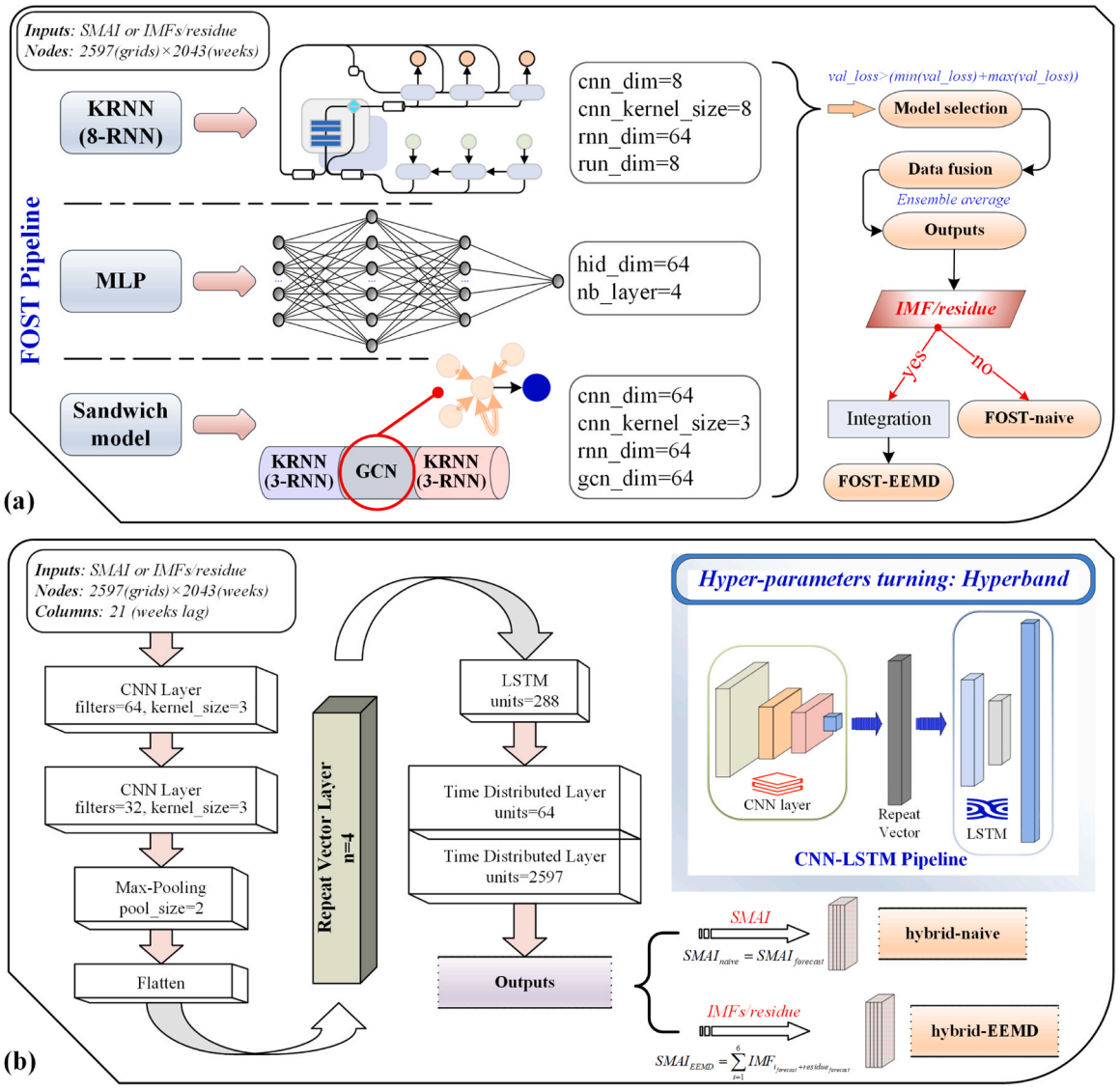

Fig. 2. Flowcharts of FOST-related framework (a) and CNN-LSTM-related model (b).

$$w_{matrix} = \begin{pmatrix} \frac{1}{|s_c - s_1|} & \frac{1}{|s_c - s_2|} & \frac{1}{|s_c - s_3|} \\ \frac{1}{|s_c - s_4|} & 0 & \frac{1}{|s_c - s_6|} \\ \frac{1}{|s_c - s_7|} & \frac{1}{|s_c - s_8|} & \frac{1}{|s_c - s_9|} \end{pmatrix} \Big/ \sum_{i=1}^{9} \frac{1}{|s_c - s_i|} \tag{3}$$

In detail, the weekly SMAI data, decomposed into 7 quantities (6 IMFs and 1 residue) with a 21-week lag series, is input separately into FOST. Simultaneously, the weekly SMAI drives its own FOST tool with parameters configured as per Fig. 2a. Following the inverse normalizing each output, predicted IMFs and residue are obtained by summing them up (labeled as FOST-EEMD), while the naive model directly produces future weekly SMAI forecasts (FOST-naive). Finally, the recurrent predictions of the future 97 weeks of SMAI are collected and compared with the SMAI dataset converted by ERA5-Land.

3.4. The hybrid CNN-LSTM model

The proposed hybrid CNN-LSTM model (Fig. 2b) is constructed using the Keras library and runs on the TensorFlow backend (Géron, 2022). This model mainly consists of Convolutional Neural Network (CNN) and Long Short-Term Memory (LSTM) layers. CNN is adept at handling data with a distinct grid-like topological structure, while LSTM excels at identifying long and short-term dependencies in data across the temporal dimension, hence the integration of CNN and LSTM aims to effectively leverage the strengths of each algorithm.

The CNN layer performs convolution operations between input data and kernels to generate new feature values, extracting spatial and temporal dependencies. Compared to other networks using matrix multiplication, the convolutional layer's reduced parameters and weight reusability are advantageous for processing image inputs. With regards to LSTM, it is fundamentally a type of RNN that overcomes the issues of gradient vanishing and exploding in traditional RNNs by "preserving memory." LSTM consists of three gates: the Input gate, the Forget gate, and the Output gate. The Input gate controls the flow of new information, the Forget gate determines how much old information to discard, and the Output gate determines the weight of retaining information in the memory cell, with values close to 1 indicating high importance and values close to 0 indicating high forgetfulness. These gates control information flow, determining old information discard, and deciding on retaining information in the memory cell.

The specific structure of drought the forecasting framework is depicted in Fig. 2b. Two convolutional layers are first added to extract

data features, followed by flattening after the max-pooling operation. The goal is to connect to the one-dimensional LSTM layer, and finally, two consecutive fully connected layers are used to map the normalized LSTM output to the desired matrix size. Dropout layers are embedded between various layers (dropout rate fixed at 0.2, meaning 20% of the output will be discarded) to avoid overfitting during the training process. In the determination of specific hyperparameters, to ensure efficient learning and performance, the optimization of hyperparameters covered by the CNN-LSTM model (such as filter size and kernel size for CNN layers, and units for LSTM) is executed using the Hyperband tool based on continuous halving search expansion (Li et al., 2017).

This framework also predicts the next four weeks of SMAI with a lag period of 21 weeks. After preprocessing the data as in FOST, normalized training samples (SMAI or individual IMF/residual) are divided into an 80% internal training set and a 20% validation set. The hyperparameter configuration is determined using Hyperband, and all separated samples are aggregated for model input with the determined parameters. Similar to FOST's nomenclature, integrated SMAI results from EEMD decomposition are labeled as "hybrid-EEMD," while directly predicted SMAI results are labeled as "hybrid-naive".

3.5. Performance evaluation

This study considers continuous and categorical statistical indicators to evaluate the reliability of experimental materials and the accuracy of prediction results.

3.5.1. Continuous metrics

The continuous metrics, including the correlation coefficient (R), root-mean-square error (RMSE), and relative bias (Rbias), are employed to pre-validate the performance of ERA5-Land records by comparing to SMCI1.0. Similarly, the forecasted SMAI undergoes verifications against the benchmark SMAI (denoted as EAR5L-SMAI) converted by ERA5-Land during the same forecasting period (March 2019 - December 2020, 97 weeks in total). The equations are as Table 2 below:where x represents the EAR5L-SMAI, y represents the forecasted-SMAI, and the overline denotes the mean values along the temporal dimension. The evaluation of the performance of each model in comparison to ERA5L-SMAI is conducted using a Taylor diagram (Taylor, 2001). This diagram provides a graphical representation of the bench and estimated data, which helps to demonstrate the relationship between the predicted and actual values. The diagram considers three statistical parameters - R, standard deviation (SD), and RMSE - to illustrate the similarity between the model predictions and the observations. The closer the points on the x-axis are to the observations, the better the agreement between the model and observations (indicating high correlation and low RMSE). Additionally, the closer the ratio of standard deviations to 1, the more consistent the model predictions are with the observations. Hence, the closer the model prediction is to the reference point in the diagram, the higher its predictive performance (Khosravi et al., 2018).

3.5.2. Categorical metrics

Recognizing that categorizing drought levels may better align with the requirements of early warning systems, therefore the categorical validation has been executed due to grading the drought (Table 1). This part introduces confusion matrix analysis to distinguish the overall agreement between the forecasts and benchmark classification. The confusion matrix consists of two dimensions: one indexed by the actual class and the other indexed by the class predicted by the classifier (in this instance, determined by the regressor). In the context of one specific drought classification, the matrix includes four key parts: True Positives (TP) values, signifying accurate predictions of drought occurrences; False Positives (FP) values, indicating instances where the drought onset is misidentified; True Negative (TN), representing correct predictions of the absence of drought; and False Negatives (FN), indicating instances where the model failed to identify the occurrence of drought.

The confusion matrix further serves to derive probability of detection (POD), false alarm rate (FAR), and critical success index (CSI). POD quantifies the likelihood that a system accurately identifies the presence of a signal or target when it exists. Conversely, FAR measures the probability of the system erroneously indicating the presence of a signal in the absence of one. Additionally, CSI serves as an encompassing metric, considering TP, FP, and FN to provide an overall assessment of classification accuracy, with a higher CSI value indicating a more successful classification performance. the equations of each metric can be computed as follow:

$$POD = \frac{TP}{TP + FN}$$
$$FAR = \frac{FP}{TP + FP} \quad (4)$$
$$CSI = \frac{TP}{TP + FN + FP}$$

In addition to using binary classification evaluation, this study also uses multi-classification evaluation to more intuitively represent the accuracy of different prediction models for the classification of drought degree. We achieve this by counting the area under the receiver operating curve (AUC-ROC) (Dikshit et al., 2021). ROC is created by plotting sensitivity (i.e., the ratio of drought levels that are correctly predicted) and on the y-axis against 1-specificity (i.e., the fractional predicted area) on the x-axis in a Cartesian coordinate system (Chen and Jin, 2022). Then a multiclass micro-averaged AUC can be directly called using the scikit-learn library on Python (Pedregosa et al., 2011), which considers the high imbalance under multi-classification conditions, for comparing the classification performance of all models. The value of AUC can be used as a basis for determining the accuracy of the classification model. The closer it is to 1, the more it means that the classification model is close to perfect, and an AUC of 0.5 means that the model fulfills only random classification.

Table 2
Continuous performance equations.

Statistical metrics	Equation	Perfect value
R	$\frac{\sum_{i=1}^{n}(x-\bar{x})(y-\bar{y})}{\sqrt{\sum_{i=1}^{n}(x-\bar{x})^2\sum_{i=1}^{n}(y-\bar{y})^2}}$	1
$Rbias$	$\frac{\sum_{i=1}^{n}(y-x)}{\sum_{i=1}^{n}(x)} \times 100\%$	0
$RMSE$	$\sqrt{\frac{\sum_{i=1}^{n}(y-x)^2}{n}}$	0

4. Results

The consistent forecasting steps from 1 to 4 weeks are for all built models, and we took subsets (16 groups in total) according to the distinct lead times for comprehensive evaluation, including forecast distribution comparison, drought events detection, and continuous and categorial validation.

4.1. Reliability evaluation of ERA5-Land soil moisture

Before initiating the assessment of the forecasting product, a preliminary comparison is conducted between the model-driven ERA5-Land soil moisture product and the SMCI1.0 data, both at their original spatiotemporal resolution of 0.1°/day.

Fig. 3 illustrates the spatial variations of continuous metrics and daily means across the study area from 2000 to 2020. The analysis reveals that ERA5-Land data exhibits notably high correlations with SMCI1.0, as indicated by R-values exceeding 0.8 over the majority of the HRB area (where the R^2 calculated by their daily means is equal to 0.83).

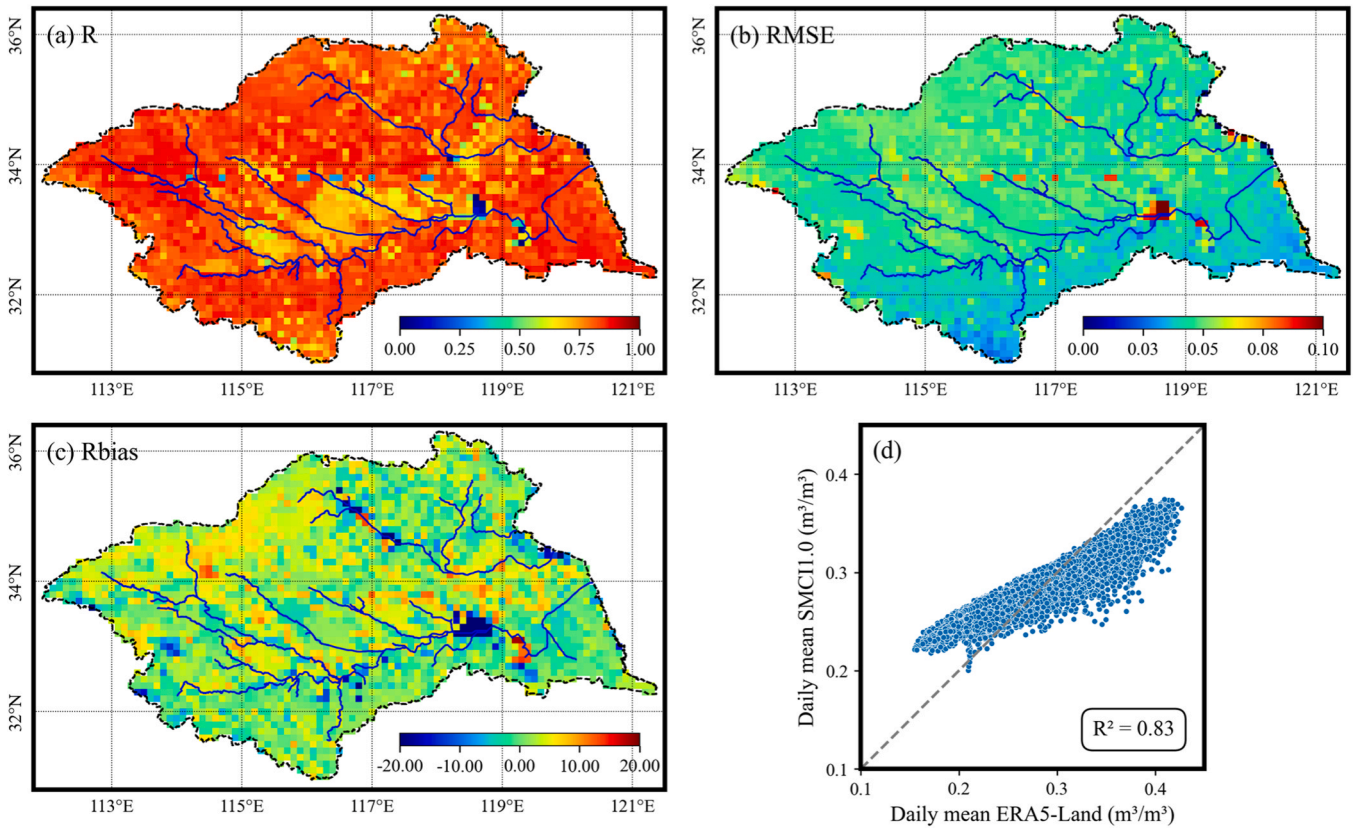

Fig. 3. Temporal R, RMSE, and Rbias distributions (a-c) over the HRB and daily basin-mean values (d) between ERA5-Land and SMCI1.0 from 2000 to 2020.

The RMSE-values map overall indicates minor spatial variability, except for relatively lower values observed in the southern part of the basin, while ERA5-Land tends to exhibit mild overestimates of SMCI soil moisture. This pre-comparison suggests that ERA5-Land closely approximates the performance of SMCI1.0, making it a viable experimental material for a long-term proxy study of soil moisture states.

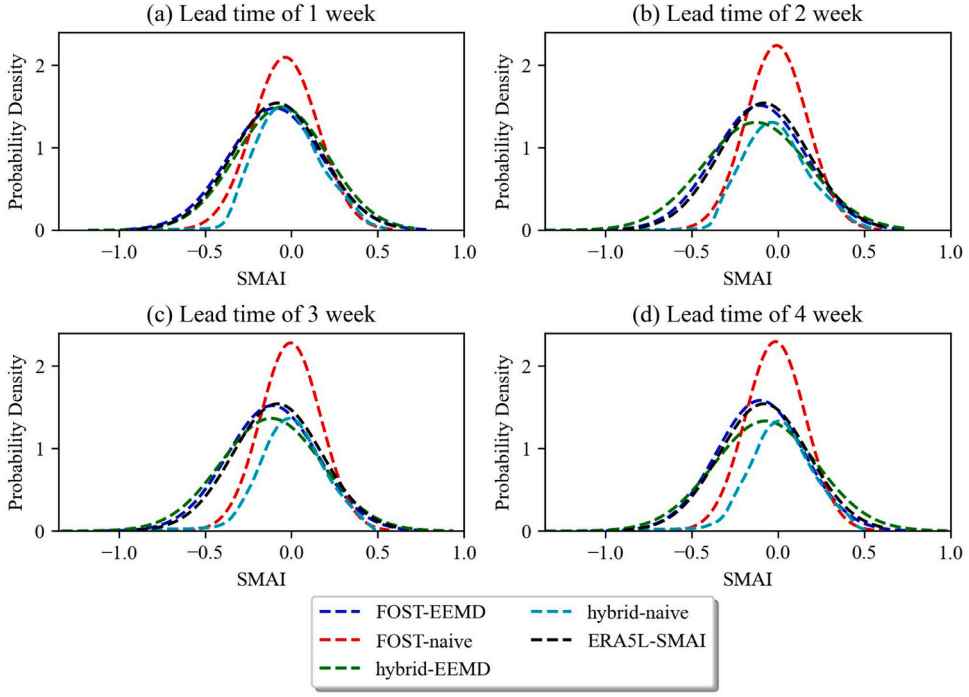

Fig. 4. PDF curves of the involved forecasting models under different lead times.

4.2. SMAI distribution and drought identification

The signature based on the soil moisture's probability density function (PDF), captures the shape of the values distribution instead of its temporal patterns (Branger and McMillan, 2020). The probability density function (PDF) of the forecasts/ERA5L-SMAI (Fig. 4) is used in this signature to describe their distribution shape, without any temporal patterns. No significant disparity among the given lead times is found, and for the same lead time, the distribution of FOST-EEMD keeps the best fit with ERA5L-SMAI, followed by hybrid-naive and hybrid-EEMD, while hybrid-naive has the worst fit. Nevertheless, a narrow-predicted interval can be detected in FOST-naive, which indicates its limited ability to predict extreme events (extreme drought or wetness).

As for the main land cover type in the study area, we extract all the grid points under the cropland mask to investigate the identification ability of different models for drought events. Fig. 5 shows the weekly series of the percentage of drought occurrences grids (SMAI < -0.05) for each model, again differentiating the lead times. FOST-EEMD follows the tendency of ERA5L-SMAI the most for all lead times, and its identification is very restrained (hardly overestimation). By contrast, other models could report much more drought events, especially during the flood season (May-September).

4.3. Continuous and categorical performance validation

4.3.1. Continuous validation statistics

The relationship between the multi-model outputs and ERA5L-SMAI is further analyzed by comparing the weekly spatial correlation and RMSE distributions. Those are displayed through a combination of spatial metrics distribution and boxplots that provide a clear depiction of the quartiles (see Figs. 6 and 7). Fig. 6 shows that the R-values for all models decline slightly with increasing lead times, with the exception of the sudden drop in FOST-naive after one-week forecasting. This drop is indicated by the steeper PDF curves and the more conservative forecast as the lead time increases.

Overall, the FOST-EEMD model obtains the best agreement with the baseline data throughout the basin with a median R and RMSE around 0.8 and 0.15 respectively. The results for the hybrid-related models are very similar, with slightly poorer correlations close to the edge for the naive model. The hybrid-EEMD model shows the largest RMSE values in the northern area compared to other models, which suggests that the EEMD technique does not significantly improve the hybrid model. A common phenomenon can be seen in all results, where the pixels labeled with a dark blue (indicating a correlation and RMSE of 0) are concentrated in the dense water system and lake areas. This is because the original ERA5 records note such pixels as constant values.

To enhance the readability of multiple statistical metrics, Taylor diagrams are utilized in this study to evaluate the performance of different models. As seen in Fig. 8, the Taylor diagrams are divided into two rows (groups), representing the grid scale and basin scale predictions, respectively.

Moving from the left to the right column, the products for 1-week forecasting periods to 4-week forecasting periods are sequentially indicated. According to the Taylor diagram interpretation, the closer the

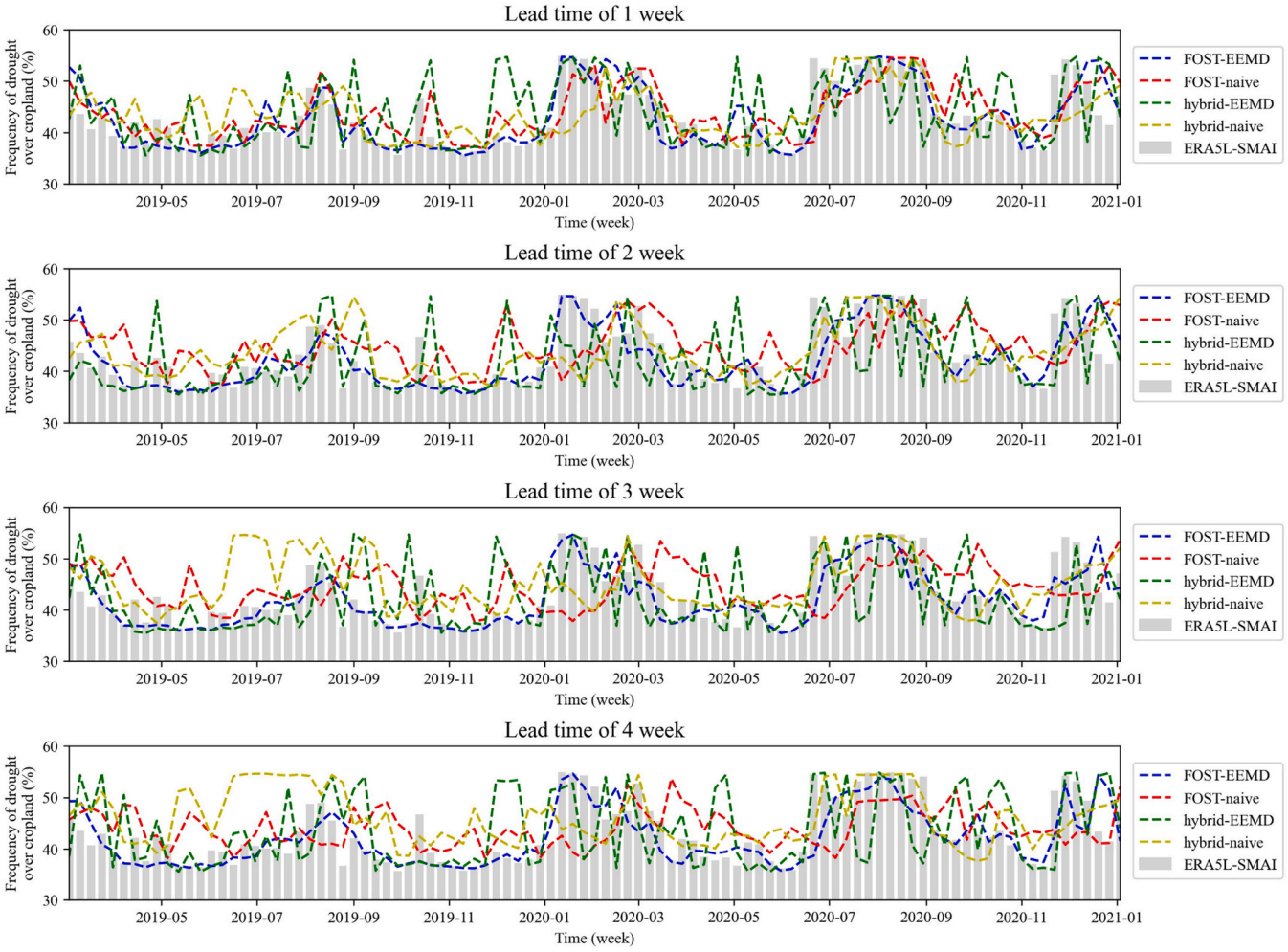

Fig. 5. Time series of area frequency defined as drought events over cropland.

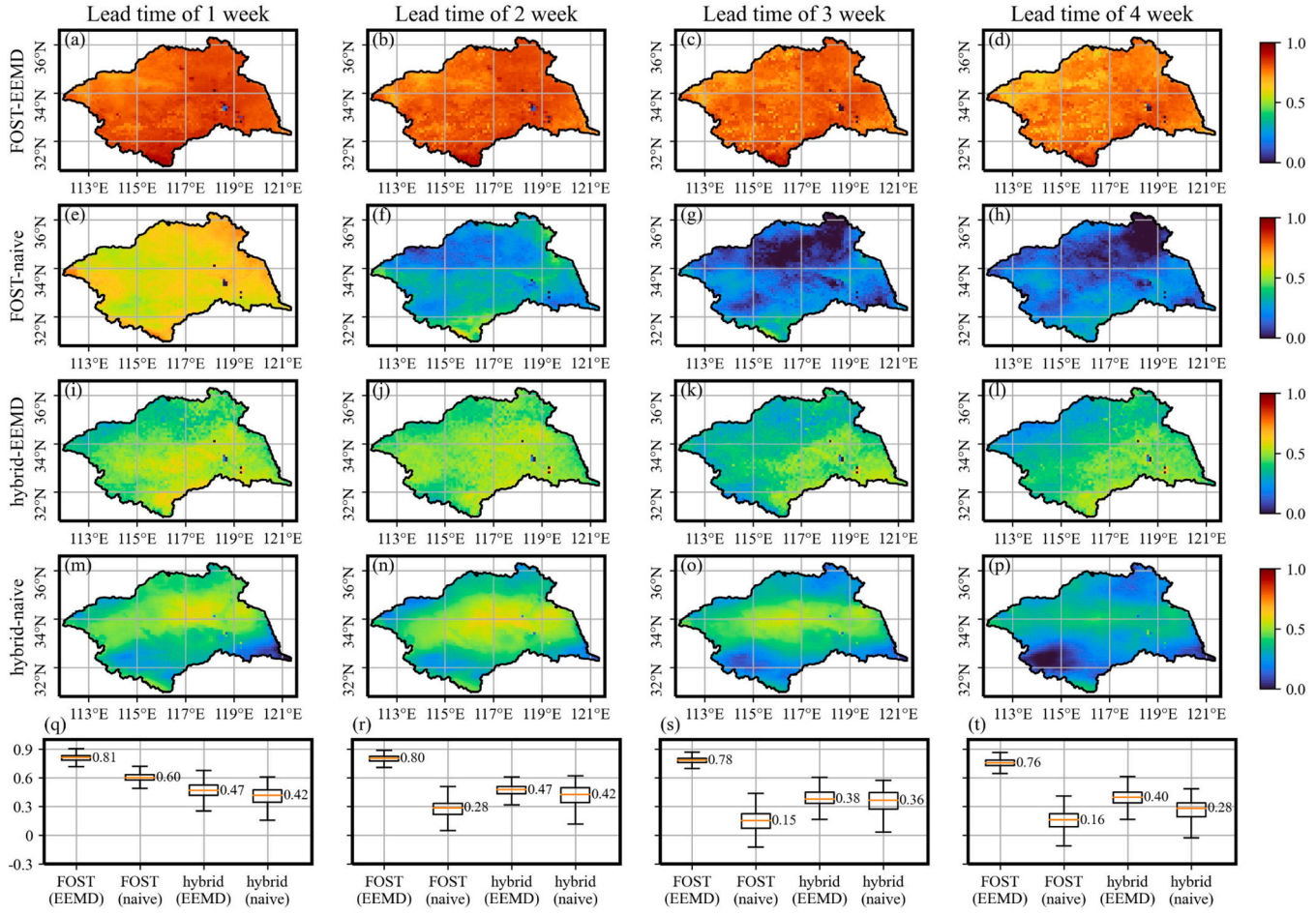

Fig. 6. Temporal R over the HRB calculated by all models with different lead times against ERA5L-SMAI over the validation period. Subfigures q-t are the boxplots of spatial indicators for each column.

model is to the black square, the better the consistency. The Taylor diagrams demonstrate that the FOST-EEMD model exhibits the best prediction capability at both grid and basin scales, unaffected by the increase in the forecasting period. This further underscores the effectiveness of the Committee model combined with EEMD in forecasting drought indices. hybrid-naive, also utilizing EEMD decomposition, maintains consistent performance regardless of spatial scale conversion, although all performance metrics at the watershed scale show a slight decrease compared to the grid scale. However, the FOST-naive and the hybrid-naive models are positioned farthest from the reference value in the Taylor diagram, implying that both models exhibit poor prediction.

Typically, such metrics at the basin scale tend to degrade compared to the grid scale due to the high spatial variability in predictive performance, as seen in Figs. 6 and 7, which demonstrate this significant variability and its impact on the poorer performance of the averaging process at the basin scale. The above results indicate that the EEMD decomposition-driven hybrid and FOST-based models provide more stable and accurate results compared to the naive models, with the FOST-EEMD model showing the most superior performance.

4.3.2. *Categorical validation statistics*

We evaluate the performance of the models in terms of grading drought classifications assigned to each forecasting set based on specific criteria (as seen in Table 1). For this purpose, three categorical statistics (POD, FAR, and CSI) corresponding with different lead times are counted between the forecasted and benchmark (ERA5L_SMAI) binary classification. In Fig. 9, the performance results are presented based on categorical statistics. Generally, all four models showed good performance in detecting the drought-free scenario at different lead times (POD ranging from 0.64 to 0.83 and CSI between 0.49 and 0.72). As expected, classification metrics generally decreased with increasing lead times, reflecting the inherent challenge of predicting indices as the temporal gap widens. However, the hybrid-naive model defied this trend in terms of POD, showcasing an improvement from 0.76 to 0.83.

In addition, the two EEMD-based models discriminated well between drought-free and severe drought scenarios for both POD (around 0.8 and 0.7) and CSI (around 0.7 and 0.5). In contrast, the very low POD-values and FAR-values of FOST-naive forecasting products indicate little skill in severe drought discrimination. Nonetheless, it is important to note the lackluster detection ability of these forecast models for mild and moderate drought scenarios, with the exception of FOST-EEMD, which is in slightly better condition, and the other forecast products basically have a POD of less than 0.3 and a CSI of less than 0.2. This may be related to the fact that the corresponding data are not sufficiently characterized in the overall distribution, leading to poor model performance in these scenarios.

The aforementioned independent statistical validation based on binary classification is insufficient to quantify the comprehensive classification ability of the forecasting system. Therefore, the ROC-AUC is introduced here to score all individual forecast products across different lead times, providing an intuitive display of the distinctive features of each model's ability to discriminate.

The micro-averaged AUC-ROC for each result is presented in Fig. 10, which includes all grids in the analysis. The FOST-EEMD model results in an AUC of 0.78, 0.77, 0.76, and 0.75 for the lead time from 1 week to 4 weeks, respectively. On the other hand, the AUC-values for other

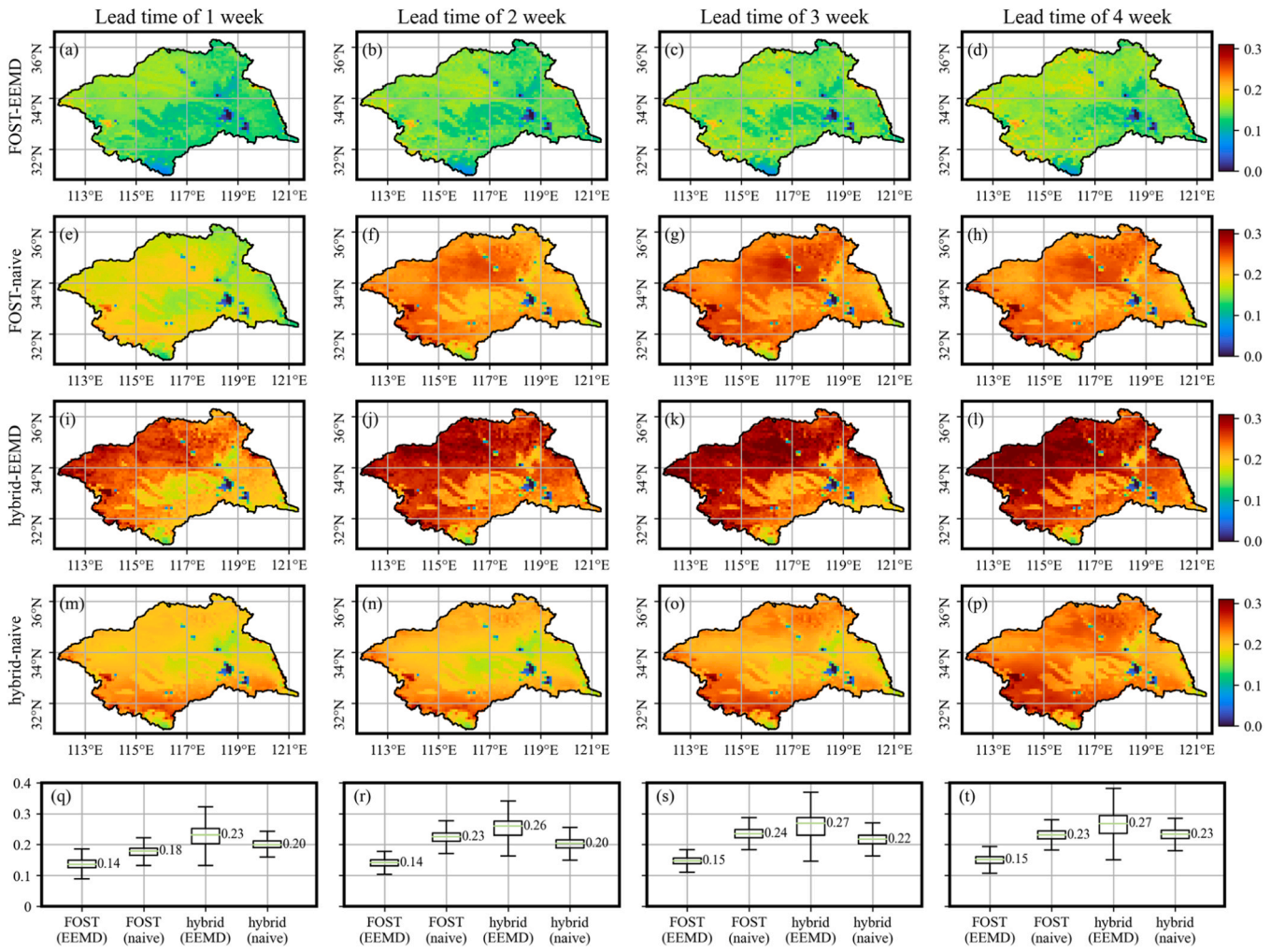

Fig. 7. Temporal RMSE over the HRB calculated by all models with different lead times against ERA5L-SMAI over the validation period. Subfigures q-t are the boxplots of spatial indicators for each column.

models range from 0.61 to 0.68, with the best performance seen in the 1-week lead results. Although the AUC values are slightly lower due to the proximity along the borderline of the drought category (Dikshit et al., 2022), all involved models reveal good classification mechanisms against the given criteria, with FOST-EEMD performing the best.

Understanding how model performance varies during transitions between dry and wet states is vital in both agricultural and environmental contexts. The "2019 China Flood and Drought Disaster Prevention Bulletin " (http://www.mwr.gov.cn/sj/tjgb/zgshzhgb/202104/t20210409_1513262.html, access date: 11–25–2023) highlights a significant drought in the Jianghuai region (which includes the HRB) from August to November 2019, characterized as a typical summer drought. In the eastern Jianghuai region, the average precipitation is 80 mm, indicating a 70% reduction from historical norms, with some areas experiencing an exceeding 80% reduction. Given the absence of detailed quantitative descriptions of the drought's evolution and intensity in the annual report, we classify grid cells with SMAI values greater than or equal to 1 as undergoing drought, while others are designated as "drought-free."

Fig. 11 shows the binary classification results for the extracted SMAI sequences of all products during the ongoing 15-week drought period (labeled with 'Dry'), along with the equivalent periods (3 weeks) before (labeled with 'Pre-dry') and after the drought (labeled with 'Post-Dry'), signifying their complete evolution of the transition between dry and wet conditions. Throughout the entire evolution, the FOST-EEMD model consistently exhibits remarkable stability, reflected in the lowest slope and nearly optimal performance with POD exceeding 0.8. In contrast, other models only demonstrate relatively uniform performance during the drought occurrence but showcase significant disparities in their "Pre-dry" and "Post-dry" performance. Notably, despite the initial struggles of hybrid-naive in effectively identifying the "Pre-dry" stage, its forecasting accuracy shows a significant upward trend with the evolving drought levels, particularly in "Post-dry" identification. Regarding the lead time, the performance of almost all models except the FOST-naive model tends to degrade to varying degrees as lead time increases, but the consistent evolution trends of metrics among each model are roughly kept across different lead times.

5. Discussion

The above work demonstrates that the framework integrated by the sequence decomposition and the committee model is a promising way of driving soil moisture for drought index forecasting. It highlights the significance of considering the specific features and operational methodologies of each module, as well as the EEMD-based enhancement in capturing and retaining historical drought information. Their combination contributes to realizing reliable and stable forecasting performance during critical phases of agricultural practice. The positive results towards FOST-EEMD validation are in varying degrees consistent with previous studies (Chatterjee et al., 2022; Esit et al., 2021; Liang and Yuan, 2021; Seo et al., 2019) demonstrating the potential of soil moisture memory in drought forecasting. In contrast, the hybrid model may

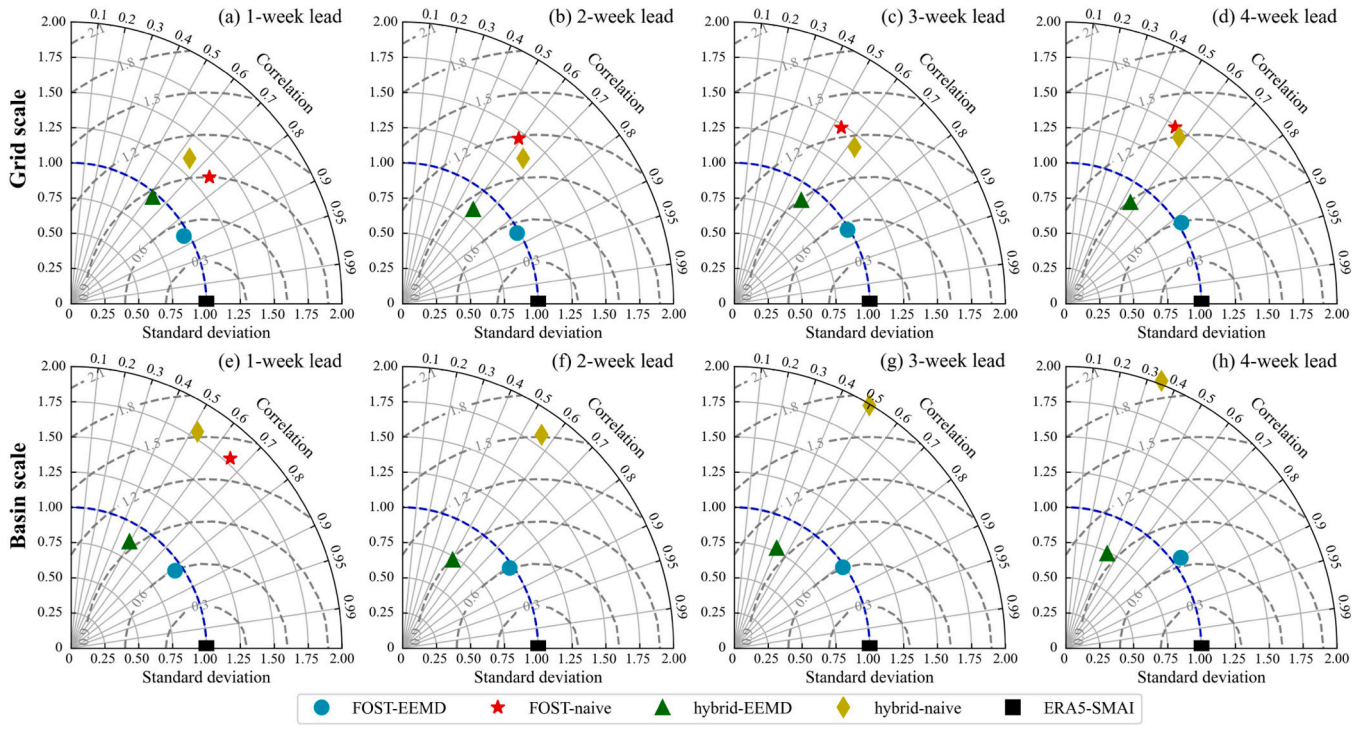

Fig. 8. Taylor diagrams for all forecasting datasets at grid scale (first row) and basin scale (second row).

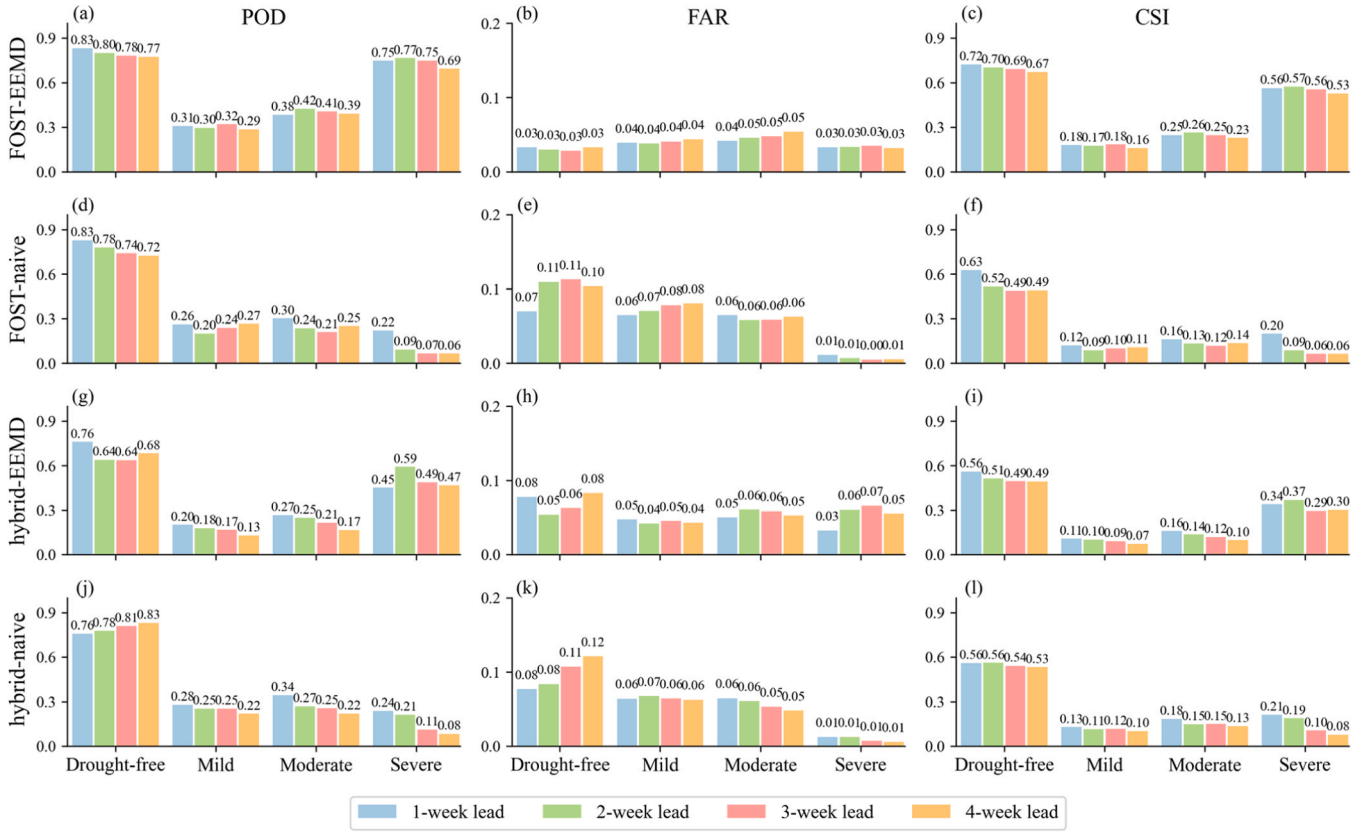

Fig. 9. Binary classification results of all forecasting datasets with different lead times under four kinds of drought conditions, columns from left to right indicate POD, FAR, and CSI, respectively.

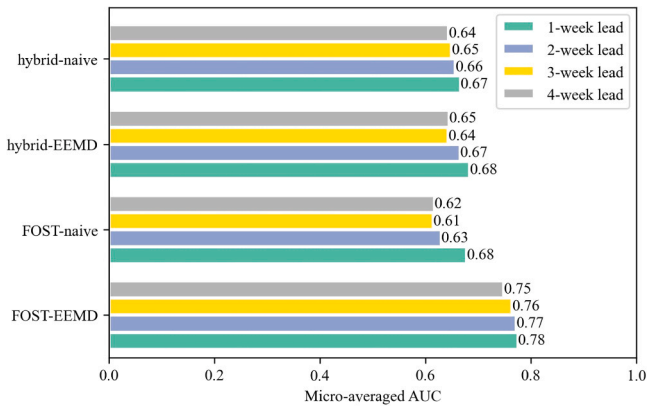

Fig. 10. AUC-ROC values of 4 classifications (drought-free condition, mild drought, moderate drought, and severe drought) among four models (FOST-EEMD, FOST-naive, hybrid-EEMD, and hybrid-naive).

not leverage these memory-enhancing features as prominently. This is related to the fact that the FOST model could discard underperforming networks during the training process based on built-in rules, while the hybrid model often has to passively accept components processed through EEMD.

Although EEMD takes a simple basic principle, it offers deep insights into the characteristics towards the required time series (Wang et al., 2015). Theoretically, a complete sifting process for EEMD stops when the obtained residue is characterized by a monotonic function, hence this characteristic of the method leaves an area for future research on determining the number of the decomposed series once served for a unified framework. Unrestricted decomposition can also be a waste of computing resources, normally it is set as Log_2N where N is the length of the total data series (Lei and Zuo, 2009) in operation, but it still generates time-consuming issues in dealing with long series over space. In stark contrast with the substantial gains observed in the committee model upon incorporating EEMD, the impact of EEMD on the hybrid model appears to be rather limited, and in fact, it may exhibit adverse effects in classification metric validations. This phenomenon could be attributed to several potential factors. First, the features extracted by EEMD may not align well with the expected input format of the hybrid model, hindering effective information transfer and integration. Second, the introduction of EEMD might introduce additional noise or complexity to the data, making the hybrid model less adaptable to such uncertainty and potentially affecting overall performance. Additionally, the hybrid model may already possess effective mechanisms for modeling time-series complexity, and the supplementary information from EEMD may not result in substantial gains, possibly introducing redundant complexity.

According to the results of binary classification validation, it is intriguing that the hybrid-naive model exhibits an enhanced detection capability for the drought-free scenario with increasing lead time. This phenomenon can be primarily attributed to the model's structural features, enabling it to capture and adapt to underlying long-term patterns and incorporate historical information. Subsequent research endeavors may explore the potential of combining this discovery with FOST-EEMD, which maintains stable performance, to mitigate the latter's performance decline in long lead time predictions. For multiclassification results, the ROC-AUC comparisons between the different prediction models show no significant differences (Fig. 8). This may be explained that SMAI values above 0.05 have wider observation intervals relative to the other categories, thus increasing the contribution to the multi-classification results. In other words, the micro-average ROC-AUC calculation aggregates the contributions of all categories to calculate the average metric (Grandini et al., 2020), while the "drought-free" category accounts for a larger number (meaning easier to classify accurately) so that contributes a larger weight than other categories, thus blurring the classification results. As drought classification is much more emphasized in effective mitigation and resource management strategies, future developments in this area may involve building sophisticated classification-based forecasting models. These models can leverage the unique strengths identified in the hybrid-naive model, particularly its improved detection capability for drought-free scenarios with extended

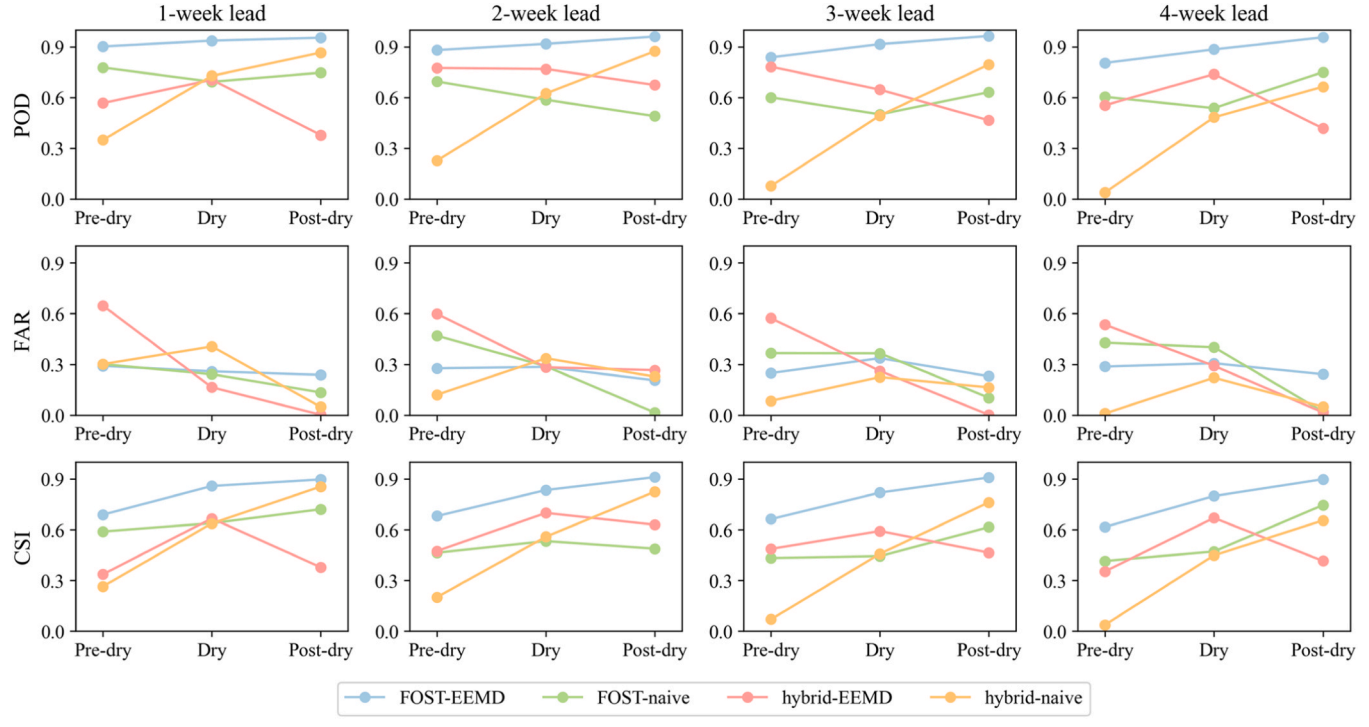

Fig. 11. Binary classification analysis of all forecasting datasets with different lead times under drought-free and drought categories. The rows represent POD/FAR/CSI, and columns represent lead times from 1 to 4 week.

lead times. Similarly, the future scope requires attention to operating models with a longer lead time and determining the point at which the skill would degrade to the level of climatology or random forecasts.

Moreover, the reason for the observed poor performance in the areas surrounding the HRB (top and bottom) for hybrid-EEMD and hybrid-naive models could be the presence of forests and urban areas (as shown in Fig. 1c), which leads to a change in the intensity of agricultural drought memory compared to a scenario dominated by croplands (AghaKouchak, 2014). Conversely, the committee model exhibits greater robustness in dealing with various land covers, partially due to the use of committees, which improve the robustness by dividing into 3 internal training and validation sets, adding spatial weights, and selecting the best model. However, this may also make it more difficult to interpret the results compared to a solo model (Khaledian and Miller, 2020).

Finally, the selection of the spatial weights matrix affects the regression results and accurate estimations significantly (Abdo et al., 2020). The FOST used in the study merely applied the same set of SMAI-based weighted assignments in each component from EEMD, whereas future practice should consider the respective spatial weights in a way of both grid values and distances. Moreover, other soil moisture-based indices, e.g. Soil Moisture Index (Hunt et al., 2009), soil moisture anomaly (Bartsch et al., 2009), and Empirical Standardized Soil Moisture Index (Carrão et al., 2016), should be involved in such frameworks to test their applicability with extending lead times. Also, the next step will calibrate the forecasts by coupling them with long-range weather forecast information (Calanca et al., 2011) and improve the temporal resolution (up to a day) of the forecasts.

6. Conclusion

In this study, we compare the performance of the committee model and the hybrid CNN-LSTM model using EEMD to demonstrate the potential of soil moisture records in forecasting the soil moisture index up to 4 weeks in advance. The results show that the committee model with FOST improves significantly with EEMD and exhibits stable positive skills for all lead times. However, this improvement is not as evident in the hybrid model. The positive results of FOST-EEMD highlight the importance of soil moisture memory in sub-seasonal drought forecasting during a crucial phase for agricultural production. As the ERA5-Land mission continues to improve, this combination could serve as a valuable tool for making agricultural drought decisions and provide a reference for numerical weather prediction model results.

CRediT authorship contribution statement

Gerald Corzo: Writing – review & editing, Writing – original draft, Validation, Supervision, Software, Resources, Project administration, Methodology, Conceptualization. **Kangmin Mao:** Software, Data curation. **Yonghua Zhu:** Resources, Data curation. **Haishen Lü:** Writing – review & editing, Supervision, Project administration, Funding acquisition, Conceptualization. **Shiliang Zhou:** Software, Resources, Data curation. **Jianbin Su:** Writing – review & editing, Supervision. **Santiago Duarte:** Writing – review & editing. **Mingwen Liu:** Resources, Data curation. **Xiaoyi Wang:** Writing – review & editing, Writing – original draft, Visualization, Validation, Software, Resources, Project administration, Methodology, Investigation, Formal analysis, Data curation, Conceptualization.

Declaration of Competing Interest

The authors declare that they have no known competing financial interests or personal relationships that could have appeared to influence the work reported in this paper.

Data Availability

Data will be made available on request.

Acknowledgments

This research is supported by the National Natural Science Foundation of China (Grant Nos. 41830752, 42101397, and 42071033). And we would like to thank the generous computer resources offered by the Snellius with a flagship cluster of Dutch supercomputing consortium.

References

Abdo, A.-B., Li, B., Zhang, X., Lu, J., Rasheed, A., 2020. Influence of FDI on environmental pollution in selected Arab countries: a spatial econometric analysis perspective. Environ. Sci. Pollut. Res. 27, 28222–28246.
Adikari, K.E., Shrestha, S., Ratnayake, D.T., Budhathoki, A., Mohanasundaram, S., Dailey, M.N., 2021. Evaluation of artificial intelligence models for flood and drought forecasting in arid and tropical regions. Environ. Model. Softw. 144, 105136.
AghaKouchak, A., 2014. A baseline probabilistic drought forecasting framework using standardized soil moisture index: application to the 2012 United States drought. Hydrol. Earth Syst. Sci. 18, 2485–2492.
Ahmed, A.A.M., Deo, R.C., Raj, N., Ghahramani, A., Feng, Q., Yin, Z., Yang, L., 2021. Deep Learning Forecasts of Soil Moisture: Convolutional Neural Network and Gated Recurrent Unit Models Coupled with Satellite-Derived MODIS, Observations and Synoptic-Scale Climate Index Data. Remote Sens. 13, 554.
Araghinejad, S., Hosseini-Moghari, S.-M., Eslamian, S., 2017. Application of data-driven models in drought forecasting. Handbook of drought and water scarcity. CRC Press, pp. 423–440.
Bartsch, A., Balzter, H., George, C., 2009. The influence of regional surface soil moisture anomalies on forest fires in Siberia observed from satellites. Environ. Res. Lett. 4, 045021.
Bergman, K.H., Sabol, P., Miskus, D., 1988. Experimental indices for monitoring global drought conditions. Proceedings of the 13th annual climate diagnostics workshop. Cambridge, MA, USA, pp. 190–197.
Branger, F., McMillan, H.K., 2020. Deriving hydrological signatures from soil moisture data. Hydrol. Process. 34, 1410–1427.
Bullinaria, J.A., 2004. Introduction to neural networks. University of Birmingham, UK.
Calanca, P., Bolius, D., Weigel, A.P., Liniger, M.A., 2011. Application of long-range weather forecasts to agricultural decision problems in Europe. J. Agric. Sci. 149, 15–22.
Carrão, H., Russo, S., Sepulcre-Canto, G., Barbosa, P., 2016. An empirical standardized soil moisture index for agricultural drought assessment from remotely sensed data. Int. J. Appl. earth Obs. Geoinf. 48, 74–84.
Chatterjee, S., Desai, A.R., Zhu, J., Townsend, P.A., Huang, J., 2022. Soil moisture as an essential component for delineating and forecasting agricultural rather than meteorological drought. Remote Sens. Environ. 269, 112833.
Chen, B., Jin, Y., 2022. Spatial patterns and drivers for wildfire ignitions in California. Environ. Res. Lett. 17, 055004.
Corzo, G., Solomatine, D., 2007. Knowledge-based modularization and global optimization of artificial neural network models in hydrological forecasting. Neural Netw. 20, 528–536.
Danandeh Mehr, A., Rikhtehgar Ghiasi, A., Yaseen, Z.M., Sorman, A.U., Abualigah, L., 2022. A novel intelligent deep learning predictive model for meteorological drought forecasting. J. Ambient Intell. Humaniz. Comput. 1–15.
Dikshit, A., Pradhan, B., Huete, A., 2021. An improved SPEI drought forecasting approach using the long short-term memory neural network. J. Environ. Manag. 283, 111979.
Dikshit, A., Pradhan, B., Assiri, M.E., Almazroui, M., Park, H.-J., 2022. Solving transparency in drought forecasting using attention models. Sci. Total Environ. 837, 155856.
Dorigo, W., de Jeu, R., Chung, D., Parinussa, R., Liu, Y., Wagner, W., Fernández-Prieto, D., 2012. Evaluating global trends (1988–2010) in harmonized multi-satellite surface soil moisture. Geophys. Res. Lett. 39.
Dorigo, W., Himmelbauer, I., Aberer, D., Schremmer, L., Petrakovic, I., Zappa, L., Preimesberger, W., Xaver, A., Annor, F., Ardö, J., Baldocchi, D., Bitelli, M., Blöschl, G., Bogena, H., Brocca, L., Calvet, J.C., Camarero, J.J., Capello, G., Choi, M., Cosh, M.C., van de Giesen, N., Hajdu, I., Ikonen, J., Jensen, K.H., Kanniah, K.D., de Kat, I., Kirchengast, G., Kumar Rai, P., Kyrouac, J., Larson, K., Liu, S., Loew, A., Moghaddam, M., Martínez Fernández, J., Mattar Bader, C., Morbidelli, R., Musial, J. P., Osenga, E., Palecki, M.A., Pellarin, T., Petropoulos, G.P., Pfeil, I., Powers, J., Robock, A., Rüdiger, C., Rummel, U., Strobel, M., Su, Z., Sullivan, R., Tagesson, T., Varlagin, A., Vreugdenhil, M., Walker, J., Wen, J., Wenger, F., Wigneron, J.P., Woods, M., Yang, K., Zeng, Y., Zhang, X., Zreda, M., Dietrich, S., Gruber, A., van Oevelen, P., Wagner, W., Scipal, K., Drusch, M., Sabia, R., 2021. The International Soil Moisture Network: serving Earth system science for over a decade. Hydrol. Earth Syst. Sci. 25, 5749–5804.
Dubois, A., Teytaud, F., Verel, S.J.C., 2021. Short term soil moisture forecasts for potato crop farming: A machine learning approach (agriculture, e.i). Comput. Electron. Agric. 180, 105902.
Esit, M., Kumar, S., Pandey, A., Lawrence, D.M., Rangwala, I., Yeager, S., 2021. Seasonal to multi-year soil moisture drought forecasting. Npj Clim. Atmos. Sci. 4, 16.

Fan, L., Xing, Z., De Lannoy, G., Frappart, F., Peng, J., Zeng, J., Li, X., Yang, K., Zhao, T., Shi, J., Others, 2022. Evaluation of satellite and reanalysis estimates of surface and root-zone soil moisture in croplands of Jiangsu Province, China. Remote Sens. Environ. 282, 113283.
Ford, T.W., Rapp, A.D., Quiring, S.M., 2015. Does Afternoon Precipitation Occur Preferentially over Dry or Wet Soils in Oklahoma? %J. J. Hydrometeorol. 16, 874–888.
Géron, A., 2022. Hands-on machine learning with Scikit-Learn, Keras, and TensorFlow. " O'Reilly Media, Inc.".
Gou, Q., Zhu, Y., Lü, H., Horton, R., Yu, X., Zhang, H., Wang, X., Su, J., Liu, E., Ding, Z., Wang, Z., Yuan, F., 2022. Application of an improved spatio-temporal identification method of flash droughts. J. Hydrol. 604, 127224.
Grandini, M., Bagli, E., Visani, G., 2020. Metrics for multi-class classification: an overview. arXiv Prepr. arXiv 2008, 05756.
He, Y., Ye, J., Yang, X., 2015. Analysis of the spatio-temporal patterns of dry and wet conditions in the Huai River Basin using the standardized precipitation index. Atmos. Res. 166, 120–128.
Hoerling, M., Eischeid, J., Kumar, A., Leung, R., Mariotti, A., Mo, K., Schubert, S., Seager, R., 2014. Causes and Predictability of the 2012 Great Plains Drought. %J. Bull. Am. Meteorol. Soc. 95, 269–282.
Hu, Y.H., Hwang, J.-N., 2002. Handbook of neural network signal processing.
Hunt, E.D., Hubbard, K.G., Wilhite, D.A., Arkebauer, T.J., Dutcher, A.L., 2009. The development and evaluation of a soil moisture index. Int. J. Climatol.: A J. R. Meteorol. Soc. 29, 747–759.
Jena, B., Saxena, S., Nayak, G.K., Saba, L., Sharma, N., Suri, J.S., 2021. Artificial intelligence-based hybrid deep learning models for image classification: The first narrative review. Comput. Biol. Med. 137, 104803.
Joksas, D., Freitas, P., Chai, Z., Ng, W.H., Buckwell, M., Li, C., Zhang, W.D., Xia, Q., Kenyon, A.J., Mehonic, A., 2020. Committee machines—a universal method to deal with non-idealities in memristor-based neural networks. Nat. Commun. 11, 4273.
Khaledian, Y., Miller, B.A., 2020. Selecting appropriate machine learning methods for digital soil mapping. Appl. Math. Model. 81, 401–418.
Khosravi, K., Mao, L., Kisi, O., Yaseen, Z.M., Shahid, S., 2018. Quantifying hourly suspended sediment load using data mining models: case study of a glacierized Andean catchment in Chile. J. Hydrol. 567, 165–179.
Koné, B.A.T., Grati, R., Bouaziz, B., Boukadi, K., 2023. A new long short-term memory based approach for soil moisture prediction. J. Ambient Intell. Smart Environ. 15, 255–268.
Lei, Y., Zuo, M.J., 2009. Fault diagnosis of rotating machinery using an improved HHT based on EEMD and sensitive IMFs. Meas. Sci. Technol. 20, 125701.
Lesk, C., Rowhani, P., Ramankutty, N., 2016. Influence of extreme weather disasters on global crop production. Nature 529, 84–87.
Li, C., Zhang, S., 2023. Synergistic changes in precipitation and soil water use efficiency and their driving mechanisms of terrestrial ecosystems in China. J. Clean. Prod. 426, 139159.
Li, L., Jamieson, K., DeSalvo, G., Rostamizadeh, A., Talwalkar, A., 2017. Hyperband: A novel bandit-based approach to hyperparameter optimization. J. Mach. Learn. Res. 18, 6765–6816.
Li, Q., Zhu, Y., Shangguan, W., Wang, X., Li, L., Yu, F., 2022c. An attention-aware LSTM model for soil moisture and soil temperature prediction. Geoderma 409, 115651.
Li, Q., Shi, G., Shangguan, W., Nourani, V., Li, J., Li, L., Huang, F., Zhang, Y., Wang, C., Wang, D., Qiu, J., Lu, X., Dai, Y., 2022a. A 1 km daily soil moisture dataset over China using in situ measurement and machine learning. Earth Syst. Sci. Data 14, 5267–5286.
Liang, M., Yuan, X., 2021. Critical role of soil moisture memory in predicting the 2012 Central United States flash drought. Front. Earth Sci. 9, 615969.
Liu, Y., Liu, Y., Wang, W., 2019. Inter-comparison of satellite-retrieved and Global Land Data Assimilation System-simulated soil moisture datasets for global drought analysis. Remote Sens. Environ. 220, 1–18.
Liu, Y., Liu, Y., Wang, W., Zhou, H., 2021. Propagation of soil moisture droughts in a hotspot region: Spatial pattern and temporal trajectory. J. Hydrol. 593, 125906.
Lorenz, D.J., Otkin, J.A., Svoboda, M., Hain, C.R., Zhong, Y., 2018. Forecasting rapid drought intensification using the Climate Forecast System (CFS). J. Geophys. Res.: Atmospheres 123, 8365–8373.
Mao, Y., Wu, Z., He, H., Lu, G., Xu, H., Lin, Q., 2017. Spatio-temporal analysis of drought in a typical plain region based on the soil moisture anomaly percentage index. Sci. Total Environ. 576, 752–765.
Meng, T., Jing, X., Yan, Z., Pedrycz, W., 2020. A survey on machine learning for data fusion. Inf. Fusion 57, 115–129.
Muñoz-Sabater, J., Dutra, E., Agustí-Panareda, A., Albergel, C., Arduini, G., Balsamo, G., Boussetta, S., Choulga, M., Harrigan, S., Hersbach, H., Others, 2021. ERA5-Land: A state-of-the-art global reanalysis dataset for land applications. Earth Syst. Sci. Data 13, 4349–4383.
Narasimhan, B., Srinivasan, R., 2005. Development and evaluation of Soil Moisture Deficit Index (SMDI) and Evapotranspiration Deficit Index (ETDI) for agricultural drought monitoring. Agric. For. Meteorol. 133, 69–88.
Otkin, J.A., Shafer, M., Svoboda, M., Wardlow, B., Anderson, M.C., Hain, C., Basara, J., 2015. Facilitating the Use of Drought Early Warning Information through Interactions with Agricultural Stakeholders. %J. Bull. Am. Meteorol. Soc. 96, 1073–1078.
Pan, Z., Ruan, X., Qian, M., Hua, J., Shan, N., Xu, J., 2018. Spatio-temporal variability of streamflow in the Huaihe River Basin, China: climate variability or human activities? Hydrol. Res. 49, 177–193.
Pedregosa, F., Varoquaux, G., Gramfort, A., Michel, V., Thirion, B., Grisel, O., Blondel, M., Prettenhofer, P., Weiss, R., Dubourg, V., et al., 2011. Scikit-learn: Machine learning in Python. the Journal of machine Learning research, 12, 2825–2830.
Prasad, R., Deo, R.C., Li, Y., Maraseni, T.J.G., 2018. Soil moisture Forecast. a Hybrid. Mach. Learn. Tech.: ELM Integr. Ensemble Empir. mode Decompos. 330, 136–161.
Prasad, R., Deo, R.C., Li, Y., Maraseni, T., 2019a. Weekly soil moisture forecasting with multivariate sequential, ensemble empirical mode decomposition and Boruta-random forest hybridizer algorithm approach. Catena 177, 149–166.
Prasad, R., Deo, R.C., Li, Y., Maraseni, T.J.C., 2019b. Weekly soil moisture forecasting with multivariate sequential, ensemble empirical mode decomposition and Boruta-random forest hybridizer algorithm approach, 177, 149–166.
Seneviratne, S.I., Corti, T., Davin, E.L., Hirschi, M., Jaeger, E.B., Lehner, I., Orlowsky, B., Teuling, A.J., 2010. Investigating soil moisture–climate interactions in a changing climate: A review. Earth-Sci. Rev. 99, 125–161.
Seo, E., Lee, M.-I., Jeong, J.-H., Koster, R.D., Schubert, S.D., Kim, H.-M., Kim, D., Kang, H.-S., Kim, H.-K., MacLachlan, C., Others, 2019. Impact of soil moisture initialization on boreal summer subseasonal forecasts: mid-latitude surface air temperature and heat wave events. Clim. Dyn. 52, 1695–1709.
Shangguan, W., Li, Q., Shi, G., 2023. A 1 km daily soil moisture dataset over China based on situ measurement (2000-2020)), in: Center, N.T.P.D. (Ed.), 1.0 ed.
Sun, P., Zhang, Q., Wen, Q., Singh, V.P., Shi, P., 2017. Multisource data-based integrated agricultural drought monitoring in the Huai River basin, China. J. Geophys. Res.: Atmospheres 122, 10–751.
Taylor, K.E., 2001. Summarizing multiple aspects of model performance in a single diagram. J. Geophys. Res.: atmospheres 106, 7183–7192.
Wang, W.-C., Chau, K.-W., Qiu, L., Chen, Y.-B., 2015. Improving forecasting accuracy of medium and long-term runoff using artificial neural network based on EEMD decomposition. Environ. Res. 139, 46–54.
Wang, X., Lü, H., Crow, W.T., Zhu, Y., Wang, Q., Su, J., Zheng, J., Gou, Q., 2021. Assessment of SMOS and SMAP soil moisture products against new estimates combining physical model, a statistical model, and in-situ observations: A case study over the Huai River Basin, China. J. Hydrol. 598, 126468.
Wu, C.L., Chau, K.W., Fan, C., 2010. Prediction of rainfall time series using modular artificial neural networks coupled with data-preprocessing techniques. J. Hydrol. 389, 146–167.
Wu, Z., Huang, N.E., 2009. Ensemble empirical mode decomposition: a noise-assisted data analysis method. Adv. Adapt. data Anal. 1, 1–41.
Wu, Z., Feng, H., He, H., Zhou, J., Zhang, Y., 2021. Evaluation of soil moisture climatology and anomaly components derived from ERA5-land and GLDAS-2.1 in China. Water Resour. Manag. 35, 629–643.
Wu, Z.-Y., Lu, G.-H., Wen, L., Lin, C.A., 2011. Reconstructing and analyzing China's fifty-nine year (1951–2009) drought history using hydrological model simulation. Hydrol. Earth Syst. Sci. 15, 2881–2894.
Yu, J., Zhang, X., Xu, L., Dong, J., Zhangzhong, L., 2021. A hybrid CNN-GRU model for predicting soil moisture in maize root zone. Agric. Water Manag. 245, 106649.
Yu, L., Li, X., Bu, K., Yan, F., Zhang, S., Liu, T., 2023. Increased background precipitation masks the moisture deficit caused by crop greening in Northeast China. J. Hydrol. 623, 129857.
Zhang, Q., Sun, P., Singh, V.P., Chen, X., 2012. Spatial-temporal precipitation changes (1956–2000) and their implications for agriculture in China. Glob. Planet. Change 82 86–95.
Zhang, Q., Yu, H., Sun, P., Singh, V.P., Shi, P., 2019. Multisource data based agricultural drought monitoring and agricultural loss in China. Glob. Planet. Change 172, 298–306.
Zhao, D., Zhang, Z., Zhang, Y., 2023. Soil Moisture Dominates the Forest Productivity Decline During the 2022 China Compound Drought-Heatwave Event, 50, e2023GL104539.
Zheng, J., Lü, H., Crow, W.T., Zhao, T., Merlin, O., Rodriguez-Fernandez, N., Shi, J., Zhu, Y., Su, J., Kang, C.S., Others, 2021. Soil moisture downscaling using multiple modes of the DISPATCH algorithm in a semi-humid/humid region. Int. J. Appl. Earth Obs. Geoinf. 104, 102530.
Zheng, J., Zhao, T., Lü, H., Shi, J., Cosh, M.H., Ji, D., Jiang, L., Cui, Q., Lu, H., Yang, K., Others, 2022. Assessment of 24 soil moisture datasets using a new in situ network in the Shandian River Basin of China. Remote Sens. Environ. 271, 112891.